Tongue Kinematics. Cortex-dependent corrections as the mouse tongue reaches for, and misses, targets

Teja Pratap Bollu[1], Sam C. Whitehead[1], Brian Kardon[1], James Redd[1], Mei Hong Liu[1], Jesse H. Goldberg[1*]

[1]Department of Neurobiology and Behavior, Cornell University, Ithaca, NY 14853.

* Corresponding author. E-mail: jessehgoldberg@gmail.com

Abstract: Precise control of the tongue is necessary for drinking, eating, and vocalizing. Yet because tongue movements are fast and difficult to resolve, neural control of lingual kinematics remains poorly understood. We combine kilohertz frame-rate imaging and a deep-learning based artificial neural network to resolve 3D tongue kinematics in mice performing a cued lick task. Cue-evoked licks exhibit previously unobserved fine-scale movements which, like a hand searching for an unseen object, were produced after misses and were directionally biased towards remembered locations. Photoinhibition of anterolateral motor cortex (ALM) abolished these fine-scale adjustments, resulting in well-aimed but hypometric licks that missed the spout. Our results show that cortical activity is required for online corrections during licking and reveal novel, limb-like dynamics of the mouse tongue as it reaches for, and misses, targets.

Main:

When you reach for an unseen object on a table in front of you, how do you move your hand to make contact? Reaches towards unseen targets exhibit variable trajectories that include initial guesses followed by 'corrective submovements' after misses (*1-4*). Sensorimotor noise reduces movement accuracy (*5*), and successfully directing submovements to a small or unseen target requires motor commands to be derived from online estimates of both current hand position and target location (*1-4*).

Many animals, including humans and rodents, have prehensile tongues that act external to the oral cavity to contact objects such as food, water and conspecifics (*6*). During natural behaviors such as licking, eating and grooming, tongues must precisely contact unseen targets. Coherent speech relies online feedback control (*7*), but it remains unknown if non vocal learners such as rodents use online control mechanisms to aim their tongues. For example when a mouse licks at an unseen water spout, does its tongue, like a hand, produce corrective submovements online after misses to zero in on the spout?

Identifying motor control principles requires precise quantification of moment-to-moment movement kinematics, but lingual kinematics are difficult to resolve because tongues are complicated, deformable effectors that move extremely fast (*6*). Even in

tractable model systems such as rodents where licking is used to study principles of motor initiation, learning, planning, and decision making (*8-14*), licks are usually measured as a binary register of whether or not a tongue contacts a spout or transects an IR beam (*8, 9*) or with single plane imaging (*10, 11*). Remarkably, it remains unclear how exactly the tongue moves during rodent licking.

To precisely resolve 3D tongue kinematics, we imaged the tongue at 1 kHz in two planes and trained a deep learning based artificial neural network (*15*) to identify and segment the tongue from side and bottom views at all phases of a lick cycle (Fig.1 A-E)(*16*). Using hull reconstruction to build a 3D model of the tongue (*17*), we estimated the tongue tip for each frame of the lick to achieve millisecond timescale resolution of the tongue tip trajectory (Fig. 1F, Sfig 1) (*16*). Mice were trained to withhold licking for at least 1 second to earn an auditory cue, and then to produce a cue-evoked lick within 1.3 seconds to earn water reward (Fig. 1A)(*16*). Cues evoked bouts of licking, as previously observed in head-fixed mouse setups where the spout could not be directly seen (Fig. 1B, Inter spout contact interval: 150ms±11ms, Inter lick interval:142±5ms, n = 9 animals) (*8, 11*). We defined 'cue-evoked licks' as licks initiated before first spout contact and 'water-retrieval licks' as licks initiated after the first tongue-spout contact in a bout (*14*)(Fig 1A, G-H).

Consistent with the idea that water-tongue contact can trigger brainstem central pattern generators (CPGs) to produce alternating phases of tongue protrusion and retraction (*18*), water-retrieval licks exhibited highly stereotyped kinematics, consisting of a single protrusion phase and a single retraction phase with no fine scale movements in between (Fig. 1G,H, Sfig. 2, Movie S1, Table 1) (*16*) (Protrusion duration, peak speed, pathlength: 32ms [30 33], 308.12 mm/s [301.60 310.95], 4.7 mm [4.59 5.29]; Retraction:32ms [32 34], 349.86 mm/s [345.63 354.66], 6.43 mm [6.43 6.49]; Latency from protrusion offset to retrieval onset: 0ms [0 0]; medians [IQRs] n = 9 animals).

In contrast to these 'water-retrieval licks', the first cue-evoked lick of a bout, initiated before spout contact, exhibited highly complex trajectories with longer durations and more acceleration peaks (Fig 1G,H, Sfig 2, Table 1)(*16*)(Durations, cued: 113ms [112 115] vs. retrieval: 70ms [69 76]; acceleration peaks, cued: 6 [5 6] vs retrieval: 4 [4 4], medians [IQR], $p<0.05$ for all comparisons, n = 9 animals, Wilcoxon signed rank test). Cued licks also exhibited significantly more trial-by-trial variability (Table 1, Sfig 2L). Examination of cued-lick trajectories revealed the utility of this complexity: during cue-evoked licks the initial tongue protrusion almost always missed the spout (Probability of contact on protrusion: 0.1±0.06, n = 9 animals, Sfig 3G). After misses, the animal initiated additional fine scale tongue movements between protrusion offset and retraction onset. These 'intra-lick movements' (ILMs) were too fast to be visually identifiable in real-time videos but were clearly visible in slow-motion (Movie S1).

When primates reach to unseen targets, corrective submovements initiated after an initial miss ensure endpoint accuracy and their number is correlated with latency to target contact (*1, 4*). Similarly, ILMs terminated at precisely clustered tongue tip

positions beneath the spout (endpoint accuracy, defined as standard deviation of the tongue tip position at moment of retraction onset across trials: 0.195±0.03 mm M/L, 0.31±0.03 mm A/P, and 0.76±0.07 mm D/V, Sfig 3 and Supplemental Text) (*16*). Further, the number of acceleration peaks per ILM strongly predicted cue-to-spout contact latencies (Sfig 4, r-square: 0.83 [0.68 0.85] , $p<0.001$, F-test, (9/9) animals) (*16*). These data show that previously unresolved tongue movements within a lick are important for making spout contact. These within lick adjustments also exhibit some phenomenological similarities to corrective submovements observed in primate reach studies (*1-4*).

Why did cue-evoked licks contain ILMs while subsequent water-retrieval ones did not? One possibility is that reduction in lick complexity is pre-programmed into the bout motor plan. Alternatively, the moment of tongue-spout contact could clarify the spout's position in space and rapidly update the next lick's motor plan, for example in the same way that even brief visual feedback at the end of a non-visually guided reach can clarify target position and increase the accuracy of a subsequent reach, obviating the need for corrective submovements (*2, 3*). Occasionally, the first one or two cue evoked licks failed to make spout contact, providing an opportunity to test how a contact affects the next lick (Probability of spout contact on first cue evoked lick: 0.63±0.08, n=9 animals). Licks preceding contact always exhibited ILMs, whereas licks following contact always lacked them, independent of when in the lick bout the first contact was made (Sfig 5, Movie S2). Thus, spout contact facilitated the transition to stereotyped and well-aimed retrieval licks, suggesting that spout contact updates the motor plan for the ensuing retrieval lick. Note that any update to an ensuing lick's motor plan must occur in the brief interval between spout contact and the ensuing protrusion onset (Latency between spout contact and subsequent protrusion: 94.5 ms [87.5 109.5], n = 9 animals). The return to variable cue-evoked licks by the next trial >1 second later also suggests that the precision of the 'memory' of spout location degrades on second timescales, as in memory-guided reach tasks (*19, 20*).

To test cortical roles in the new kinematics we describe, we used VGAT-hChR2-EYFP mice to photoinactivate anterolateral (ALM) or posterior (PMM) motor cortical areas (*16*), two non-overlapping regions with functional projections to brainstem lingual circuits (*8, 18*)(Fig 2A). Photoinhibition of ALM, but not PMM, impaired spout contact (Fig 2B, Sfig 6, Probability of contact: Intact: 1 [1 1] vs ALM inactivated: 0.03 [0.03 0.13] $p<0.05$, n = 9 animals, Wilcoxon signed rank test; probability of contact, Intact: 1 [1 1] vs PMM inactivated: 1 [1 1] $p>0.05$, n = 9 animals, Wilcoxon signed rank test), consistent with previous studies (*9, 13*).

To test why ALM inactivations impaired tongue-spout contact we analyzed tongue kinematics during ALM-inactivated trials, first focusing on the ability of the cue to cause tongue protrusion. ALM inactivation reduced the probability of tongue protrusion, consistent with the idea that ALM sends movement initiation signals to brainstem circuits to initiate a cued lick bout (*8, 9, 13, 18*). However, cue-evoked protrusions were

mostly intact following ALM inactivation, even in cases where spout contact was not (Fig 2b, Movie S3)(Probability of protrusion, Intact:1 [0.9968 1] vs Inactivated: 0.58 [0.58 0.61], $p<0.05$, n = 9 animals, Wilcoxon signed rank test). Tongue protrusions initiated during ALM inactivation exhibited similar latencies and peak speeds as control trials (Fig 2D,L-N, Table 2; Latency to protrusion, Intact:103 [93 114] vs ALM Inactivated:132 [122 140]; Protrusion peak speed, Intact:195.45 mm/s [191.22 199.37] vs ALM Inactivated:186.15 mm/s [181 191.54], $p>0.05$, n = 9 animals, Wilcoxon signed rank test). Thus deficient lick initiation did not fully explain ALM inactivation-associated deficits in spout contact.

Why did cue-evoked licks during ALM inactivation fail to make spout contact even on trials when protrusion was normal? Cued licks initiated with ALM inactivated exhibited significantly shorter durations, reduced speeds, reduced pathlengths and fewer acceleration peaks (Fig. 2, Table 2; Intact Duration, Acceleration peaks: 113ms [112 115], 6 [5 6]; ALM Inactivated: 53ms [51 58], 2 [2 3], $p<0.05$ all comparisons, n=9 animals, Wilcoxon signed rank test). ALM photoinhibition also reduced trial-by-trial variability of lick kinematics (*16*)(Table 2). Critically, on ALM inactivated trials, mice failed to produce ILMs after protrusions and immediately retracted the tongue (Duration of ILM on missed spout contact, Intact: 50 ms [40 57] vs ALM Inactivated: 0ms [0 0], $p<0.05$, n = 9 animals, Wilcoxon signed rank test). On rare cases where spout contact occurred during ALM photoinhibition, subsequent water retrieval licks were not strongly affected by ongoing ALM inactivation (Supplemental Text, Table 4, and SFig 7). Thus, with ALM inactivated, animals could usually generate cued licks but could not make within-lick adjustments that facilitate spout contact. Within-reach adjustments in primates also rely on cortical activity (*21-23*).

We next trained mice to lick to left or right by differential placement of a single spout across distinct daily sessions (*16*). High success rates showed that cue-evoked licks could be directed towards remembered spout locations (Spout-Left, Probability of Success:1 [1 1], Latency to Spout Contact: 213±19 ms, n=9 animals; Spout-Right, Probability of Success:1 [1 1], Latency to Spout Contact: 232±22 ms, n=7 animals). Kinematic analyses of cue-evoked licks revealed that the tongue protrusions were significantly biased towards whichever spout location was rewarded in the session (Fig. 3, Movie S4, Median Lateral Displacement: 0.55mm [0.50 0.60] (left), and -0.27[-0.15 -0.33] mm (right), $p<0.05$ one sided t-test for all measures, n = 9 and 7 animals respectively).

To test if directionally biased tongue protrusion required cortex, we inactivated ALM or PMM after mice learned to lick at left or right spouts. Consistent with past work and with lick-straight conditions (*9*), inactivation of ALM, but not PMM, reduced cue-evoked spout contact (Probability of spout contact, Spout left, Intact: 1 [1 1] vs ALM Inactivated: 0.57 [0.54 0.67]; Spout right, Intact: 1 [1 1] vs ALM Inactivated: 0.47 [0.3 0.66], $p<0.05$,n = 9 and 7 animals, Wilcoxon signed rank test). Kinematic analysis revealed, however, that tongue protrusions were still usually present during ALM

photoinhibition (Probability of protrusion with ALM inactivation, left: 0.85 [0.53 0.86], right: 0.67 [0.54 0.81], n=7 and 9 animals, respectively, medians [IQRs]) and that protrusions remained significantly biased toward the remembered spout location (Fig 3, Movie S5, Median Lateral Displacement (ALM inactivated): 0.49±0.14 mm(left) $p<0.05$, -0.21± 0.07mm (right) $p<0.05$, and 0.004±0.07mm (center) $p>0.05$, n = 9, 7 and 9 animals respectively, one sided t-test for all measures). As with spout straight-conditions, ALM inactivated trials lacked the ILM component of the lick (Spout left, Duration of ILM, Intact 9ms [4 15] vs ALM inactivated 0 [0 0]; Spout right, Intact: 14ms [8 19] vs Inactivated: 3ms [0 7], $p<0.05$, n = 9 and 7 animals respectively,Wilcoxon signed rank test), resulting in a failure to make online adjustments important for spout contact.

During reaching, primates use online proprioceptive feedback and estimates of target position to aim corrective submovements towards unseen targets (*1, 24*). To test if ILMs were random walk-like movements or if they were aimed in prefered directions, we examined the distribution of each ILM's initial velocity vector (*16*). In all mice and in all sessions, ILMs were strongly biased in specific directions (Fig 4A,D,G Insets, $p<0.001$ chi square test for a uniform distribution. 12/12 animals) (*16*). This ILM directional bias could in principle be due to a further extension of the preceding protrusion or could be an aimed re-direction towards a target. Surprisingly, within sessions, the direction of each ILM's initial velocity vector was not correlated with the direction of the immediately preceding protrusion (linear regression of protrusion direction vs ILM direction, $p>0.05$ for 12/12 animals, F-test) (*16*), suggesting that a new direction command was generated at the moment of protrusion offset. To test if this direction was biased towards remembered spout locations, we computed a direction bias, defined as the dot product between each ILM's initial velocity vector and the three vectors from ILM starting position to the three possible target locations (left, center, or right) (targets defined as the median tongue tip position at spout contact)(*16*) (Supplemental Text, Fig 4b and SFig 3D-F). Across mice and sessions, the ILMs' initial velocity vectors were significantly more biased towards the rewarded target location (Fig. 4, Table 5), consistent with online aiming that may account for both current and target tongue position. Yet importantly, ILMs were highly tortuous (ILM tortuosity: 1460 mm-3 [740 2378]; straight line tortuosity: 0)(*16*), suggesting that the consequence of ILM aiming was to bias a noisy and/or exploratory process.

ALM is implicated in both lick planning and execution (*8, 9, 13*). In our task, which by design only focused on execution, we found that deficits during ALM inactivation were primarily attributable to an inability to produce within-lick adjustments, and to a lesser extent, the inability to initiate a lick. These results predict that placing the spout very close to the mouth could rescue ALM-inactivation associated execution deficits. Experiments confirmed this prediction (SFig 8, Probability of contact, spout Close: Intact: 1 [1 1] vs ALM inactivated: 0.93 [0.72 0.96] $p<0.05$, n = 9 animals, Wilcoxon signed rank test), supporting the more general idea that motor cortical activity in mice is critical for online adjustments but not for cue-evoked movement initiation (*25*).

High speed videography has repeatedly overturned assumptions of lingual control in bats, hummingbirds, chameleons and cats (*26-29*). By combining kilohertz frame-rate imaging and deep learning based machine vision methods, we tracked the rodent tongue in 3D for the first time and discovered that licks cannot be explained by open loop central pattern generators that drive simple binary ballistic events. Instead, individual licks exhibit complex, variable trajectories with limb-like dynamics, including the production of motor cortex-dependent online adjustments that facilitate target contact.

Precise aiming of the human tongue is necessary for coherent speech and can be leveraged for prosthetic control (*7, 30*). Our discovery of cortex-dependent corrections during licking establishes an experimentally tractable system for dissecting mechanisms of online motor control and reveals common principles underlying limb and lingual control

References

1. D. E. Meyer, R. A. Abrams, S. Kornblum, C. E. Wright, J. Keith Smith, Optimality in human motor performance: ideal control of rapid aimed movements. *Psychological review* **95**, 340 (1988).
2. W. A. Spijkers, P. Lochner, Partial visual feedback and spatial end-point accuracy of discrete aiming movements. *J Mot Behav* **26**, 283-295 (1994).
3. M. A. Khan, I. M. Franks, Online versus offline processing of visual feedback in the production of component submovements. *J Mot Behav* **35**, 285-295 (2003).
4. C. Ghez, J. Gordon, M. F. Ghilardi, R. Sainburg, in *"Contributions of Vision and Proprioception to Accuracy in Limb Movements," in The cognitive neurosciences,* M. S. Gazzaniga, Ed. (The MIT Press, Cambridge, MA, US, 1995), chap. 35, pp. 549-564.
5. A. A. Faisal, L. P. Selen, D. M. Wolpert, Noise in the nervous system. *Nat Rev Neurosci* **9**, 292-303 (2008).
6. W. M. Kier, K. K. Smith, Tongues, tentacles and trunks: the biomechanics of movement in muscular-hydrostats. *Zoological journal of the Linnean Society* **83**, 307-324 (1985).
7. F. H. Guenther, Speech sound acquisition, coarticulation, and rate effects in a neural network model of speech production. *Psychol Rev* **102**, 594-621 (1995).
8. T. Komiyama *et al.*, Learning-related fine-scale specificity imaged in motor cortex circuits of behaving mice. *Nature* **464**, 1182-1186 (2010).
9. M. J. Goard, G. N. Pho, J. Woodson, M. Sur, Distinct roles of visual, parietal, and frontal motor cortices in memory-guided sensorimotor decisions. *Elife* **5**, (2016).
10. J. P. Welsh, E. J. Lang, I. Suglhara, R. Llinás, Dynamic organization of motor control within the olivocerebellar system. *Nature* **374**, 453 (1995).
11. M. A. Gaffield, J. M. Christie, Movement rate is encoded and influenced by widespread, coherent activity of cerebellar molecular layer interneurons. *Journal of Neuroscience* **37**, 4751-4765 (2017).
12. S. Crochet, S. H. Lee, C. C. H. Petersen, Neural Circuits for Goal-Directed Sensorimotor Transformations. *Trends Neurosci* **42**, 66-77 (2019).

13. K. Svoboda, N. Li, Neural mechanisms of movement planning: motor cortex and beyond. *Current opinion in neurobiology* **49**, 33-41 (2018).
14. L. T. Coddington, J. T. Dudman, The timing of action determines reward prediction signals in identified midbrain dopamine neurons. *Nat Neurosci* **21**, 1563-1573 (2018).
15. O. Ronneberger, P. Fischer, T. Brox, U-net: Convolutional networks for biomedical image segmentation. *International Conference on Medical image computing and computer-assisted intervention*, 234-241 (2015).
16. *Materials and methods are available as supplementary materials on Science Online.*
17. T. Beatus, J. M. Guckenheimer, I. Cohen, Controlling roll perturbations in fruit flies. *J R Soc Interface* **12**, (2015).
18. L. E. McElvain *et al.*, Circuits in the rodent brainstem that control whisking in concert with other orofacial motor actions. *Neuroscience* **368**, 152-170 (2018).
19. J. McIntyre, F. Stratta, F. Lacquaniti, Viewer-centered frame of reference for pointing to memorized targets in three-dimensional space. *J Neurophysiol* **78**, 1601-1618 (1997).
20. M. Heath, D. A. Westwood, Can a visual representation support the online control of memory-dependent reaching? Evident from a variable spatial mapping paradigm. *Motor Control* **7**, 346-361 (2003).
21. A. P. Georgopoulos, J. F. Kalaska, R. Caminiti, J. T. Massey, Interruption of motor cortical discharge subserving aimed arm movements. *Exp Brain Res* **49**, 327-340 (1983).
22. A. S. Dickey, Y. Amit, N. G. Hatsopoulos, Heterogeneous neural coding of corrective movements in motor cortex. *Front Neural Circuits* **7**, 51 (2013).
23. B. Rohrer *et al.*, Movement smoothness changes during stroke recovery. *J Neurosci* **22**, 8297-8304 (2002).
24. C. Ghez, J. Gordon, M. F. Ghilardi, Impairments of reaching movements in patients without proprioception. II. Effects of visual information on accuracy. *J Neurophysiol* **73**, 361-372 (1995).
25. M. Heindorf, S. Arber, G. B. Keller, Mouse Motor Cortex Coordinates the Behavioral Response to Unpredicted Sensory Feedback. *Neuron* **99**, 1040-1054 e1045 (2018).
26. A. Rico-Guevara, M. A. Rubega, The hummingbird tongue is a fluid trap, not a capillary tube. *Proceedings of the National Academy of Sciences* **108**, 9356-9360 (2011).
27. C. J. Harper, S. M. Swartz, E. L. Brainerd, Specialized bat tongue is a hemodynamic nectar mop. *Proceedings of the National Academy of Sciences* **110**, 8852-8857 (2013).
28. P. M. Reis, S. Jung, J. M. Aristoff, R. Stocker, How cats lap: water uptake by Felis catus. *Science* **330**, 1231-1234 (2010).
29. J. H. de Groot, J. L. van Leeuwen, Evidence for an elastic projection mechanism in the chameleon tongue. *Proceedings of the Royal Society of London. Series B: Biological Sciences* **271**, 761-770 (2004).
30. J. Kim *et al.*, The tongue enables computer and wheelchair control for people with spinal cord injury. *Sci Transl Med* **5**, 213ra166 (2013).

Acknowledgments:

We thank Joe Fetcho, Melissa Warden, Neville Hogan and members of the Goldberg lab for comments on the manuscript. We thank Bilal Bari for valuable advice on behavioral training, and Nikil Prasad and Jackson Walker for technical advice and support. **Funding:** Funding to JHG was provided by the NIH (grant # DP2 HD087952), the Dystonia Medical Research Foundation, the Pew Charitable Trust and the Klingenstein Neuroscience Foundation. **Author contributions**: TB and JHG designed the research; TB performed the experiments; TB, SW, JR and JHG analyzed the data; BK, TB and JHG built hardware, ML and TB performed surgeries and histology; TB, SW and JHG wrote the paper. The authors declare no competing financial interest.

Table S1. Kinematics of Cue Evoked and Water Retrieval Licks

Cue-evoked and water retrieval licks had distinct kinematics both at the complete trajectory level and when segmented into lick phases. * denotes a $p<0.05$ for a Wilcoxon paired-rank test between cue-evoked and retrieval licks, n = 9 animals.

	Cue-Evoked Lick		Retrieval Lick	
	Median	IQR [25% 75%]	Median	IQR [25% 75%]
Kinematics of complete lick trajectory				
Acceleration peaks*	6	[5 6]	4	[4 4]
Duration* (s)	113	[112 115]	70	[69 76]
Peak Speed* (mm/s)	316.86	[276.40 317.28]	351.26	[350.49 353.90]
Pathlength* (mm)	9.53	[9.11 10.20]	11.41	[11.08 11.80]
Entropy of complete lick trajectory				
Acceleration peaks*	2.05	[1.54 2.19]	1.39	[1.28 1.52]
Duration*	2.88	[2.71 3.00]	1.88	[1.80 2.07]
Peak Speed	2.95	[2.93 2.98]	2.77	[2.76 2.81]
Pathlength*	2.22	[2.12 2.34]	1.80	[1.61 1.91]
Kinematics by Lick Phase				
Duration (ms)				
Protrusion	33	[30 36]	32	[30 33]
ILM*	42	[26 53.5]	0	[0 0]
Retraction*	28	[27 29]	32	[32 34]
Speed (mm/s)				
Protrusion*	195.45	[191.22 199.37]	308.12	[301.60 310.95]
Retraction*	316.61	[270.12 316.86]	349.86	[345.63 354.66]
Pathlength (mm)				
Protrusion*	3.77	[3.40 3.78]	4.70	[4.59 5.29]
Retraction*	4.76	[4.67 4.80]	6.43	[6.43 6.49]

Table S2. Kinematics of Cue Evoked Licks with ALM inactivation

ALM inactivation altered the kinematics of cue-evoked licks both at the complete trajectory level and when segmented into lick phases. * denotes a p<0.05 for a Wilcoxon paired-rank test between cue-evoked and retrieval licks, n = 9 animals.

	Cue-Evoked Lick (Intact)		Cue-Evoked Lick (ALM Inactivated)	
	Median	IQR [25% 75%]	Median	IQR [25% 75%]
Kinematics of complete lick trajectory				
Acceleration peaks*	6	[5 6]	2	[2 3]
Duration* (ms)	113	[112 115]	51	[51 58]
Peak Speed (mm/s)	316.86	[257.10 329.98]	209.81	[209.81 301.67]
Pathlength* (mm)	9.53	[9.11 10.20]	5.99	[5.99 6.35]
Entropy of complete lick trajectory				
Acceleration peaks*	2.05	[1.54 2.16]	1.25	[1.12 1.59]
Duration*	2.88	[2.71 3.00]	1.94	[1.75 1.95]
Peak Speed	2.95	[2.85 3.04]	2.25	[1.60 2.58]
Pathlength*	2.22	[2.12 2.34]	2.71	[2.51 2.72]
Kinematics by Lick Phase				
Duration (ms)				
Protrusion*	33	[30 36]	23	[22 26]
ILM*	42	[26 53.50]	0	[0 0]
Retraction*	28	[27 29]	25	[24.5 26]
Speed (mm/s)				
Protrusion	195.45	[191.22 199.37]	191.54	[181.00 191.54]
Retraction*	316.61	[270.12 316.86]	250.81	[238.67 250.81]
Pathlength (mm)				
Protrusion*	3.77	[3.40 3.78]	2.74	[2.48 2.74]
Retraction*	4.76	[4.67 4.80]	3.24	[3.21 3.24]

Table S3. Kinematics of Cue Evoked Licks with PMM inactivation

PMM inactivation did not alter the kinematics of cue-evoked licks both at the complete trajectory level and when segmented into lick phases. * denotes a p<0.05 for a Wilcoxon paired-rank test between cue-evoked and retrieval licks, n = 9 animals.

	Cue-Evoked Lick (Intact)		Cue-Evoked Lick (PMM Inactivated)	
	Median	IQR [25% 75%]	Median	IQR [25% 75%]
Kinematics of complete lick trajectory				
Acceleration peaks	5	[5 5]	6	[5 6]
Duration	98	[88 105.5]	91.50	[88.00 107.00]
Peak Speed	328.71	[309.43 332.95]	330.66	[314.07 334.24]
Pathlength	9.44	[9.15 9.60]	9.06	[9.03 10.11]
Entropy of complete lick trajectory				
Acceleration peaks	1.63	[1.44 1.86]	1.55	[1.46 1.90]
Duration*	2.41	[2.17 2.78]	2.26	[2.21 2.60]
Peak Speed*	3.13	[3.13 3.14]	2.76	[2.76 2.87]
Pathlength*	2.42	[2.37 2.58]	2.32	[2.04 2.41]
Kinematics by Lick Phase				
Duration (ms)				
Protrusion	36	[33 37]	36.5	[36 38]
ILM	31	[28 32]	26.5	[24.50 32]
Retraction	28.5	[27 30]	28	[28 30]
Peak Speed (mm/s)				
Protrusion	209.18	[204.81 211.98]	222.43	[198.60 240.12]
ILM	53.62	[47.45 69.40]	52.77	[44.91 61.80]
Retraction	332.29	[307.88 332.30]	329.47	[313.40 331.53]
Pathlength (mm)				
Protrusion	4.00	[3.83 4.08]	3.93	[3.84 4.29]
ILM	1.34	[0.83 1.65]	1.32	[0.79 1.35]
Retraction	4.33	[4.30 4.44]	4.54	[4.54 4.75]

Table S4. Kinematics of Retrieval Licks with ALM inactivation

ALM inactivation made the water-retrieval licks hypmetric. * denotes a p<0.05 for a Wilcoxon paired-rank test between cue-evoked and retrieval licks, n = 9 animals.

	Retrieval Lick (Intact)		Retrieval Lick (ALM Inactivated)	
	Median	IQR [25% 75%]	Median	IQR [25% 75%]
Kinematics of complete lick trajectory				
Acceleration peaks	4	[3 4]	3	[3 3]
Duration* (ms)	69	[63 76]	60	[59 62.0]
Peak Speed (mm/s)	350.54	[325.59 351.26]	330.76	[314.75 356.33]
Pathlength* (mm)	11.47	[11.08 11.77]	9.48	[7.60 10.18]
Kinematics by Lick Phase				
Duration (ms)				
Protrusion*	33	[30 35]	31	[29 32]
ILM	0	[0 0]	0	[0 0]
Retraction*	32	[32 35]	29	[27.50 31]
Peak Speed (mm/s)				
Protrusion	308.12	[301.60 310.95]	303.57	[303.57 303.57]
Retraction	349.86	[345.63 354.66]	317.87	[301.54 319.72]
Pathlength (mm)				
Protrusion*	4.70	[4.59 5.29]	3.95	[3.43 3.98]
Retraction*	6.43	[6.43 6.49]	5.54	[4.33 5.61]

Methods

Animals and Surgery

All experiments were carried out in accordance with NIH guidelines and were approved by the Cornell Institutional Animal Care and Use Committee. 12 VGAT-Chr2-EYFP (Jackson laboratory, JAX Stock #014548) animals of ages 32-52 were individually housed under a 12hr light/dark cycle for the duration of the study, and were tested during the dark phase. On days when mice weren't being trained or tested, mice received 1 ml of water. Mice were trained and tested in experimental sessions that lasted 0.5h to 1h. If the mice did not receive at least 1 ml of water in the behavioral session, their water was supplemented to meet the 1ml/day requirement.

Under isoflourane induced anesthesia, all animals were implanted with 400um, 0.43NA cannulas (Thorlabs) bilaterally over ALM (2.5 A/P, ±1.5 ML) and PMM (0.5 A/P ± 1.5 M/L). Mice were also implanted with a custom modified RIVETS headplate for head restraint during the behavioral sessions (*31*).

Behavioral Setup

To simultaneously image two orthogonal planes of the mouse's orofacial movements, we placed a mirror (Thorlabs ME1S-P01 1") angled at 45 degrees below the mouse's mouth. We used a Phantom VEO 410L camera with a Nikon 105mm f/2.8D AF Micro-Nikkor lens to acquire videos with a resolution of 192x400 pixels at 1000 fps. Custom Labview code for behavioral training was run on a training system built using a National Instruments sbRIO-9636 FPGA.

Behavioral Training

Five days after surgery and postoperative recovery, mice were started on water restriction. Mice were restricted to 1 mL of water per day and their body weight was recorded daily. The behavioral training began after mice reached a steady state of body mass of 80% original body weight with water restriction. Mice typically reached the steady state body weight in 5-6 days. In the first behavioral sessions, mice were head restrained and water (3ul) was delivered paired with an auditory cue (3.5 kHz). The spout was placed directly ahead of the mouse, approximately 1.6 mm from the mouse's incisors. The auditory cues had an inter trial interval with an exponential distribution, this provided a flat hazard rate such that the probability of a cue was not altered over the duration of the trial. After the mice learned to reliably lick the spout following the auditory cue, in subsequent sessions water delivery was made contingent on spout contact happening within 1.3 seconds of the auditory cue. Once the mice learned to initiate spout contact following an auditory cue to dispense water, we imposed a 1 second no spout contact window prior to the onset of the auditory cue. If the animal made spout contact within this window, the inter trial interval was extended by an interval randomly drawn from the exponential distribution. This discouraged mice from spontaneously licking the spout and ensured that the licking we observed was in response to the auditory cue. Once the animals were trained, in separate sessions ALM or PMM were pseudo randomly photoinhibited bilaterally in 15% of the trials. After photoinhibition experiments were completed with the spout straight at 1.6 mm, the spout location was moved to 3.2 mm from the mouse's incisors. Once the mouse learned to lick the spout at 3.2 mm, pseudorandom bilateral ALM or PMM

inactivations were again performed. Once the animal learned to lick left or right, pseudorandom bilateral ALM or PMM inactivations were again performed.

Photoinhibition

We used Laser LED light sources (LDFLS_450-450, Doric Life Sciences Ltd), attached to an optical rotary joint (FRJ_1×2i_FC-2FC_0.22) and delivered light to the implanted cannulas using 400um, 0.43NA lightly armored metal jacket patch cords. The light sources were set to analog input mode and driven with a sinusoidal pulse (40 Hz, 10mW peak, 0.75 s duration)(*32*).

Artificial Deep Neural Network for Segmentation

We used an implementation of a semantic segmentation neural network (U-NET) to identify and segment the tongues from high speed videography. U-Net uses a contracting path that is thought to identify context, i.e. “is the tongue present in this image?”, and a symmetric expanding path that precisely localizes the relevant object, i.e “where is the tongue present in the image?”

U-NET Architecture. The contracting path of the network was constructed as a series of 5 repeating modules. Each module was an application of two 3x3 convolutions, with each convolution followed by a ReLU and 2x2 max pooling operation with stride 2 for downsampling. At each downsampling, the number of feature channels was doubled. The number of channels for the first module was 2, and thus for the remaining modules they were 4,8,16 and 32 respectively. Dropout of 0.7 was added at the output of module 4 and 5. The expanding path of the network was symmetric to the contracting path, it had 4 repeating modules. Each module had: First, a 3x3 convolution with half the number of channels from the previous module. Second, an upsampling step that doubled the frame size. Third, a concatenation step that merged the output of the current module with that of the symmetric module from the contracting path. And Finally, two 3x3 convolutions, with each convolution followed by a ReLU. The last layer of the network was a 1x1 convolution layer that followed the last layer of the expanding path. This network had a sigmoid activation function and gave the probability of an individual pixel being a part of the tongue.

Network training. The network was trained on 3668 frames pseudo randomly selected from the dataset of 25,258,017 frames from all 12 animals across all sessions. The training set was balanced such that half of the 3668 frames had the mouse tongue visible. The frames were then manually annotated with both the side view and the bottom view using a custom GUI for labelling. A separate network was trained for the side and bottom views. The networks were trained with a batch size of 256 images, using the adam optimizer and a binary cross entropy loss function. The networks were trained till the loss function reached an asymptotic value, of 0.0047 for the side view network and 0.0023 for the bottom view network, with a validation accuracy of 0.9979 and 0.9991 respectively. Both networks reached asymptotic performance within 4000 epochs.

Extracting 3D tongue kinematics

To obtain the full 3D kinematics of the tongue tip during a lick bout, we performed a visual hull reconstruction using two orthogonal views (bottom and right side) of the tongue filmed via high-speed videography. This hull reconstruction procedure is contingent upon crisp 2D silhouettes of the tongue from both the bottom and side views, which were obtained by U-NET segmentation. We next constructed a 3D voxel representation of the tongue by identifying voxels that map onto the tongue silhouette when projected back into the 2D image space. Intuitively, this can be thought of as placing the bottom and side view images on adjacent faces of a cube, projecting the silhouettes in towards the center of the cube, and identifying the 3D intersection of these projections (SFig 1A). For trials in which the side view of the tongue tip is occluded by the lick spout, we estimate the shape of the occluded tongue region by fitting a cubic spline to the boundary of the side silhouette and extrapolating the boundary spline into the occluded region.

We obtained 3D coordinates of the tongue centroid by averaging, and then defined the tongue tip as the position on the tongue that is furthest from the centroid in the direction of the lick, which we located using a two-step search process (Sfig 1B)(*17*). In the first step, we define an initial search vector, which points forward (anterior) and down (ventral) from the tongue centroid. This initial search vector is used across all videos. Using this initial search vector, we identify voxels in the tongue hull that satisfy the search criteria of i) the vector connecting the voxel to the centroid makes an angle of less than 45 degrees with the initial search vector and ii) the distance from the centroid to the voxel is $\geq$75% of all voxel-to-centroid distances. We take the collection of voxels that satisfy these criteria, which we call candidate voxels, and calculate their mean location. The unit vector between the tongue centroid and the mean location of the candidate voxels was then used as the search vector for the second step of the search process, as it points in the rough direction of tongue tip. The second step of the search process follows a similar pattern to refine the search described above. Using the refined search vector from step one, we perform a search for voxels that are i) within a given angular range (15 degrees) of the search vector and ii) are located on the boundary of the tongue hull. The average location of this second set of candidate voxels is defined to be the tongue tip (SFig 1C). The resultant 3D kinematics for the tongue tip were filtered using a 8 pole, 50 Hz low-pass filter.

Trajectory Analysis

Tongue volume was determined from the convex hull reconstruction from the segmented images (see “Extracting 3D tongue kinematics”). Tongue tip trajectories were segmented into three distinct phases on the basis of the rate of volume change of the tongue. The protrusion phase was defined as the time from when the tongue is detected upto the first minimum in the rate of volume expansion of the tongue. The retraction phase was defined as the time from the last minima of the rate of volume expansion of the tongue until the tongue was back in the mouse’s mouth. Movements between the end of protrusion and the onset of retraction were defined as intra lick movements (ILM).

Instantaneous speed was calculated as a one-sample difference of the position vector and pathlength was calculated as the cumulative sum of the one-sample difference of the position vector over the entire trajectory. Acceleration was calculated as the one sample-difference of the instantaneous speed. Peaks were identified using the findpeaks function in MATLAB. Lateral displacement was defined as the distance of the tip position from the midline

of the mouse. The midline of the mouse was defined as the line that passes through the point equidistant between the mice's nostrils and the midpoint of the mouse's incisors. Tortuosity was calculated as the integral of square of derivative of curvature, divided by the length of a curve. Intuitively, this formulation describes the degree to which the curvature of a trajectory changes relatively to its length. This formulation establishes that the tortuosity of a circle or a straight line is zero.

Direction bias was estimated as the dot product of the initial ILM direction vector and either the Target direction vector or the simulated off-target direction vector. The ILM direction vector was defined as the direction vector from the location of the tongue tip at the onset of the ILM to the location of the tongue tip at the first speed minimum. The Target direction vector was defined as the direction vector from the location of the tongue tip at the onset of the ILM to the median location of the tongue tip at retraction onset in that session. Similarly, the simulated off-target direction vector was defined as the direction vector from the location of the tongue tip at the onset of the ILM to the simulated target locations in that session.

Since targets were changed across sessions and not within sessions, and not all mice were trained in all directions, the simulated off-target direction vectors were defined as follows. For the left sessions: The center/straight simulated target had the same the A/P location and was on the midline. The right simulated target had the same A/P location as the target, and symmetrical M/L location from the midline for e.g. if the left target was at +4mm A/P and +1.2 mm M/L, the right simulated target would be at +4mm A/P -1.2mm M/L and the center straight target would be at +4mm A/P 0 M/L. For the right sessions: symmetrical to the left sessions. For the center sessions: Both the right and left simulated targets had the same A/P location, and M/L was ± 1.2 mm.

Statistical Analyses

For measures of central tendency, we used medians and interquartile ranges (IQR) since these measures do not assume normality of distributions. They are represented as medians [IQR]. For e.g. a duration measure of 18ms [16 22], represents a median of 18ms with interquartile range from 16ms to 22ms.

Statistical analyses were performed using standard tests in MATLAB, including one sided t-tests, two-sample t-tests and Wilcoxon signed-rank tests. Correlation was tested in by applying the F-test statistic to a linear fit. A chi-square goodness of fit test was performed to determine if a distribution was uniform.

Supplementary Text

The position of the tongue tip at the moments of retraction onset and spout contact

During prehension, rodents and primates position do not aim their fingertips to directly contact an object; rather, they precisely position their fingers so that an object can be well retrieved upon grasp (*33*). Mice also did not contact the spout with the tips of their tongues; instead, at the moment of spout contact the tongue tip was always beneath the spout; contact at this position appeared to enhance water retrieval by the dorsal tongue surface (Sfig 3)(Movie S1). Interestingly, the tongue tip positions at the moment of spout contact were strikingly stereotyped within animals, but could vary across animals (endpoint accuracy at spout contact (cue-evoked): 0.195±0.03 mm M/L, 0.31±0.03 mm A/P, and 0.76±0.07 mm D/V, endpoint accuracy at spout contact (retrieval): 0.17±0.03 mm M/L, 0.32 ±0.09mm A/P, and 0.53±0.13 mm D/V), suggesting that each animal had a preferred 'target' location for spout contact.

Effect of ALM inactivation on retrieval licks

Both ALM inactivated cued-licks and normal water retrieval-licks lacked ILMs and exhibited highly stereotyped trajectories, suggesting that ALM photoinhibition simply transformed cue-evoked licks into water-retrieval licks. Yet a critical difference was that ALM inactivated licks were reliably hypometric and rarely reached the spout (Probability of contact, Intact Water Retrieval: 0.91±0.09 vs ALM inactivated Cue Evoked: 0.12±0.10, $p<0.01$, n= 9 animals, Wilcoxon signed rank test)(Fig. 2B, N). Rare spout contacts during ALM inactivation provided an opportunity to examine how ongoing photoinhibition affected subsequent water retrieval licks that always followed (Probability that a successful cue-evoked lick with ALM inactivated was followed by another protrusion: 1 [1 1], n = 9 animals). ALM inactivation only subtly reduced the pathlength and the duration of these retrieval licks, and did not affect their peak speed or the number of acceleration peaks (Table 4 and SFig 7)

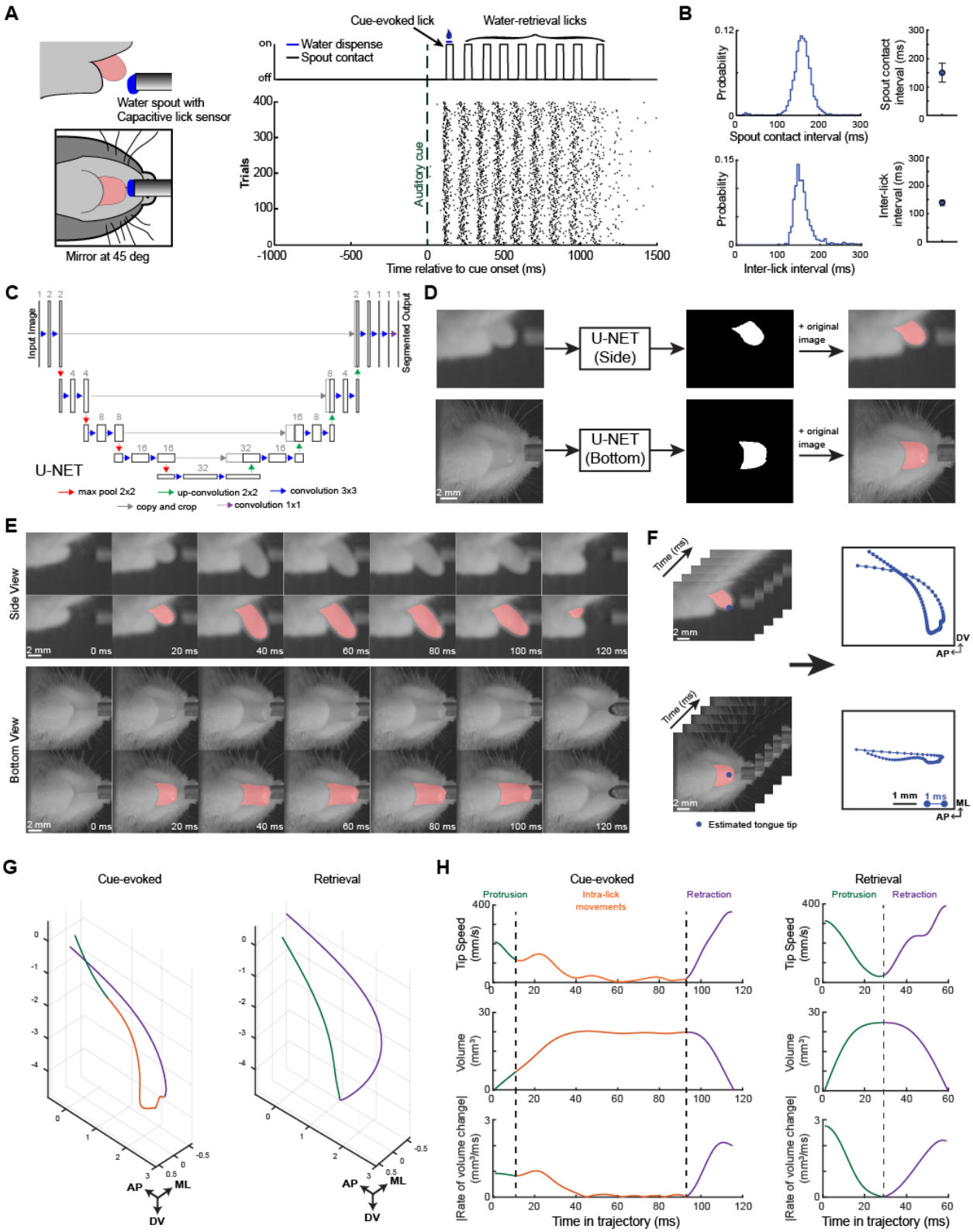
A
Water spout with
Capacitive lick sensor
Mirror at 45 deg
Cue-evoked lick
Water-retrieval licks
on
off
Water dispense
Spout contact
Trials
Auditory cue
Time relative to cue onset (ms)
B
Probability
Spout contact interval (ms)
Inter-lick interval (ms)
C
Input Image
Segmented Output
U-NET
max pool 2x2
up-convolution 2x2
convolution 3x3
copy and crop
convolution 1x1
D
U-NET (Side)
U-NET (Bottom)
+ original image
2 mm
E
Side View
Bottom View
0 ms
20 ms
40 ms
60 ms
80 ms
100 ms
120 ms
F
Time (ms)
DV
AP
ML
1 mm
1 ms
Estimated tongue tip
G
Cue-evoked
Retrieval
AP
ML
DV
H
Protrusion
Intra-lick movements
Retraction
Tip Speed (mm/s)
Volume (mm³)
|Rate of volume change| (mm³/ms)
Time in trajectory (ms)

Fig. 1 Machine vision based tracking of lingual kinematics identifies intra-lick movements important for spout contact.

A) Left, the tongue was filmed at kilohertz framerate in two planes (from the side and, via a mirror, from the bottom) during a cued lick task. Right, spout contacts as a function of time for a single trial (top) and lick raster showing spout contact onset times across 400 trials (bottom). Water was dispensed at the moment of first spout contact. We defined cue-evoked licks as those initiated before first spout contact in a trial and water-retrieval licks as ones initiated after.

B) Left: Distributions of Inter-spout contact intervals (top) and and inter tongue protrusion intervals (bottom) for a single mouse. Right: Median+/-Interquartile interval values across 9 mice.

C) Architecture of the artificial neural network (U-NET) used to segment the tongue from the background image. U-Net has characteristic symmetrical contraction and expansion paths that simultaneously capture localization and image context. Each box corresponds to a multi-channel feature map and numbers above each layer indicate the the number of channels; color-coded arrows indicate sequential processing steps.

D) Pipeline for tongue segmentation. Left to right, top: side view of the tongue as the input image to U-NET, the identified tongue mask, and the mask plus the input image. Bottom: process is repeated separately for the bottom view of the tongue.

E) Example frames from side and bottom views across a single lick cycle. Each row shows the raw image above the image overlaid with the U-net labeled tongue mask.

F) Tongue tip positions, computed from a 3d tongue model (Sfig. 1), were estimated in each frame (left) , resulting in millisecond timescale tracking of tongue tip in two planes

G) Trajectories from two planes were converted into a 3-D trajectory of a single cue-evoked lick (left) and water-retrieval lick (right). Protrusion, retraction, and intra-lick movement phases of the lick are labeled in green, purple and orange, respectively.

H) Top to bottom: Tip speed, tongue volume, and absolute value of rate of tongue volume change for the cue-evoked and retrieval licks shown in G. Protrusion offsets and retraction onsets were defined as the first and last minima in the rate of volume change (vertical dotted lines). Note that the cue-evoked lick contained ILMs (orange) between protrusion offset and retraction onset, whereas retrieval licks exhibited a single minimum in rate of volume change, marking the transition from protrusion to retraction.

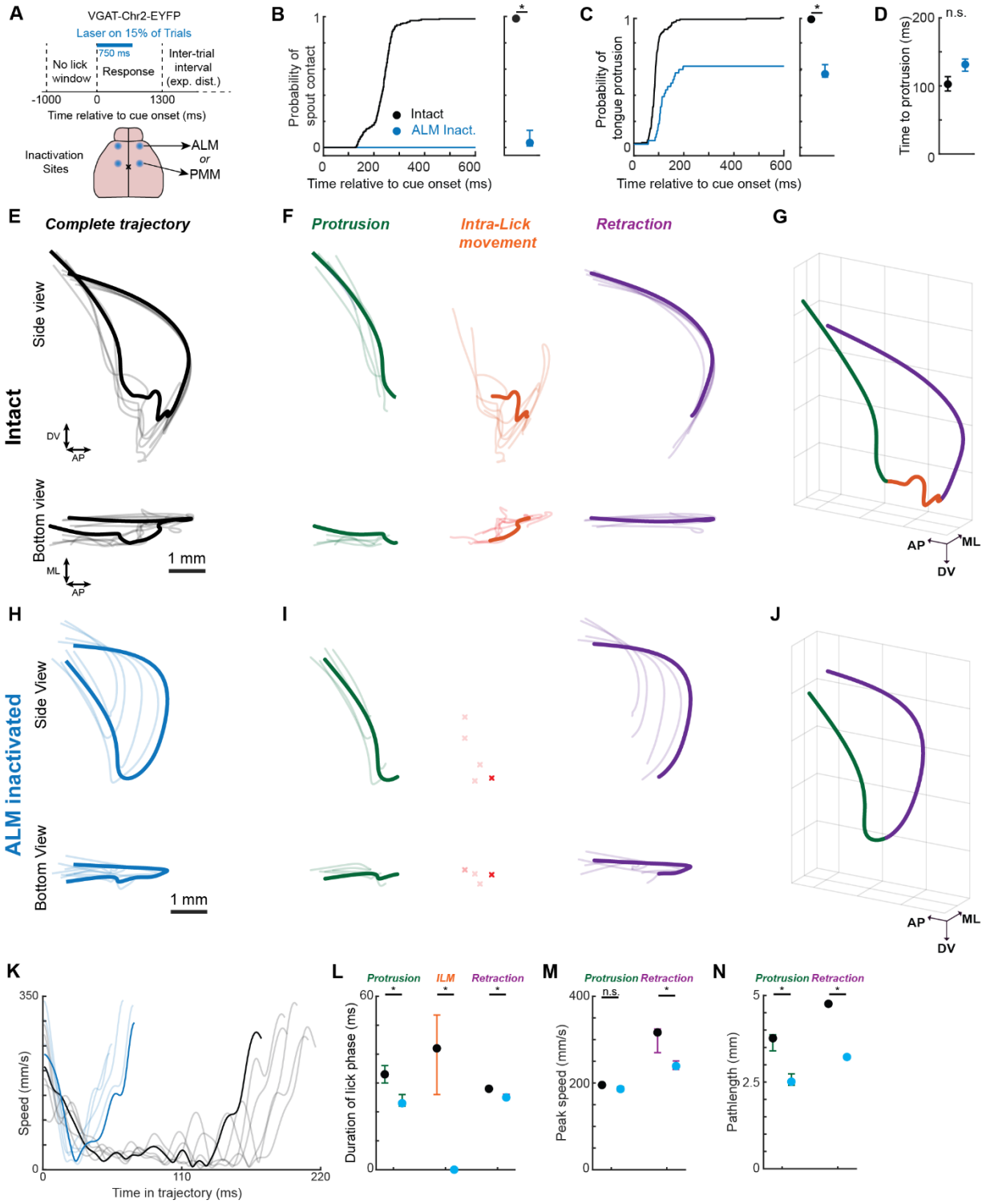
A
VGAT-Chr2-EYFP
Laser on 15% of Trials
750 ms
No lick window
Response
Inter-trial interval (exp. dist.)
-1000
0
1300
Time relative to cue onset (ms)
Inactivation Sites
ALM
or
PMM
B
Probability of spout contact
Intact
ALM Inact.
Time relative to cue onset (ms)
C
Probability of tongue protrusion
Time relative to cue onset (ms)
D
Time to protrusion (ms)
n.s.
E
Complete trajectory
Intact
Side view
Bottom view
DV
AP
ML
1 mm
F
Protrusion
Intra-Lick movement
Retraction
G
AP
ML
DV
H
ALM inactivated
Side View
Bottom View
1 mm
I
J
AP
ML
DV
K
Speed (mm/s)
Time in trajectory (ms)
L
Protrusion
ILM
Retraction
Duration of lick phase (ms)
M
Protrusion
Retraction
n.s.
Peak speed (mm/s)
N
Protrusion
Retraction
Pathlength (mm)

Fig. 2. Photoinactivation of ALM impairs spout contact by abolishing intra-lick movements.
A) ALM or PMM were bilaterally photoinactivated on 15% of randomly interleaved trials.
B) Cumulative probability of tongue-spout contact relative to cue onset during laser-off and ALM-photoinactivated trials. Right, median +/- IQR probability of spout contact within a trial across mice (n=9 mice).
C) Data plotted as in B for onsets of tongue protrusions.
D) Median latency from cue onset to tongue protrusion onset across animal (errorbars, IQRs, n=9 mice)
E-G) Laser off trials. E) Six overlaid tongue tip trajectories during cue-evoked licks. A single lick is bold for clarity. F) Protrusion, intra-lick, and retraction phases of the trajectories from E are separately plotted. G) 3-D trajectory of the highlighted lick shown in E-F.
H-J) data plotted as in E-G for 6 tongue trajectories from ALM photoinactivated trials. Red X symbols denote the absence of ILMs.
K) Speed versus time for the tongue trajectories shown in E,H. Blue, ALM inactivated.

L-N) Median durations (L), Peak speeds (M) and Pathlengths (N) of lick phases with ALM intact (black) and ALM Inactivated (blue). (median +/- IQRs).

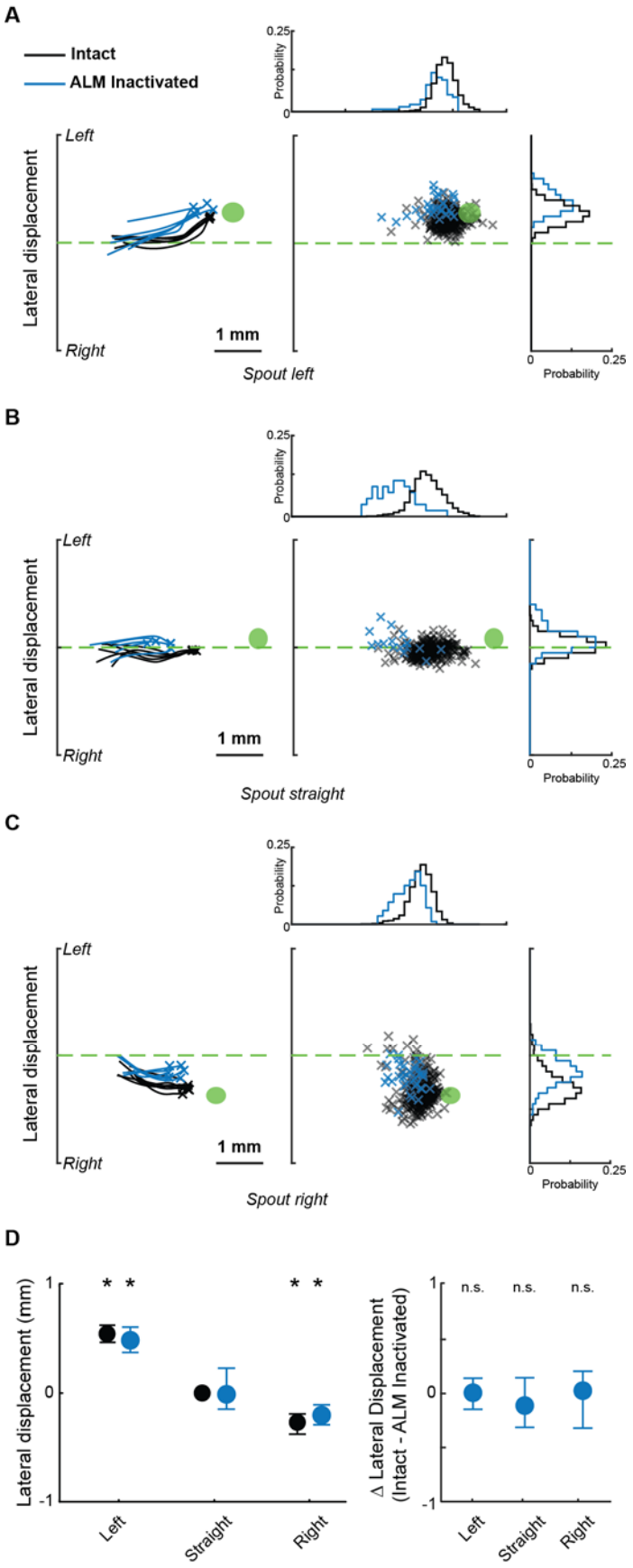
A
Intact
ALM Inactivated
Probability
0.25
0
Left
Right
Lateral displacement
1 mm
Spout left
B
Spout straight
C
Spout right
D
Lateral displacement (mm)
1
0
-1
* *
n.s.
Left
Straight
Right
Δ Lateral Displacement
(Intact - ALM Inactivated)

Fig. 3. Directionally biased tongue protrusions persist during ALM inactivation.
A) Left: Five example tongue protrusions (from bottom view) from a single session with the spout placed to the left (blue, ALM inactivated; black: ALM intact). Green ellipse denotes 95% CI of the tongue tip location at the moment of retraction onset. Center: Scatter plot of tongue tip positions at the end tongue protrusions. Probability distributions of the ALM intact (black) and inactivated (blue) dots are projected along the axes at top and right (binsize, 120um). Green line, midline.
B-C) Data plotted in A for sessions with centered (B) and right (C) spout placements.
D) Left: The lateral placement of the tongue tip at the moment of protrusion offset is plotted across left, straight, and right sessions (black: laser off; Blue: ALM Inactivated; data are median+/-IQR across n=9 animals). Right: The average difference in lateral displacement between ALM intact and ALM inactivated trials (Median+/- IQR displacements across animals (n=7 mice)

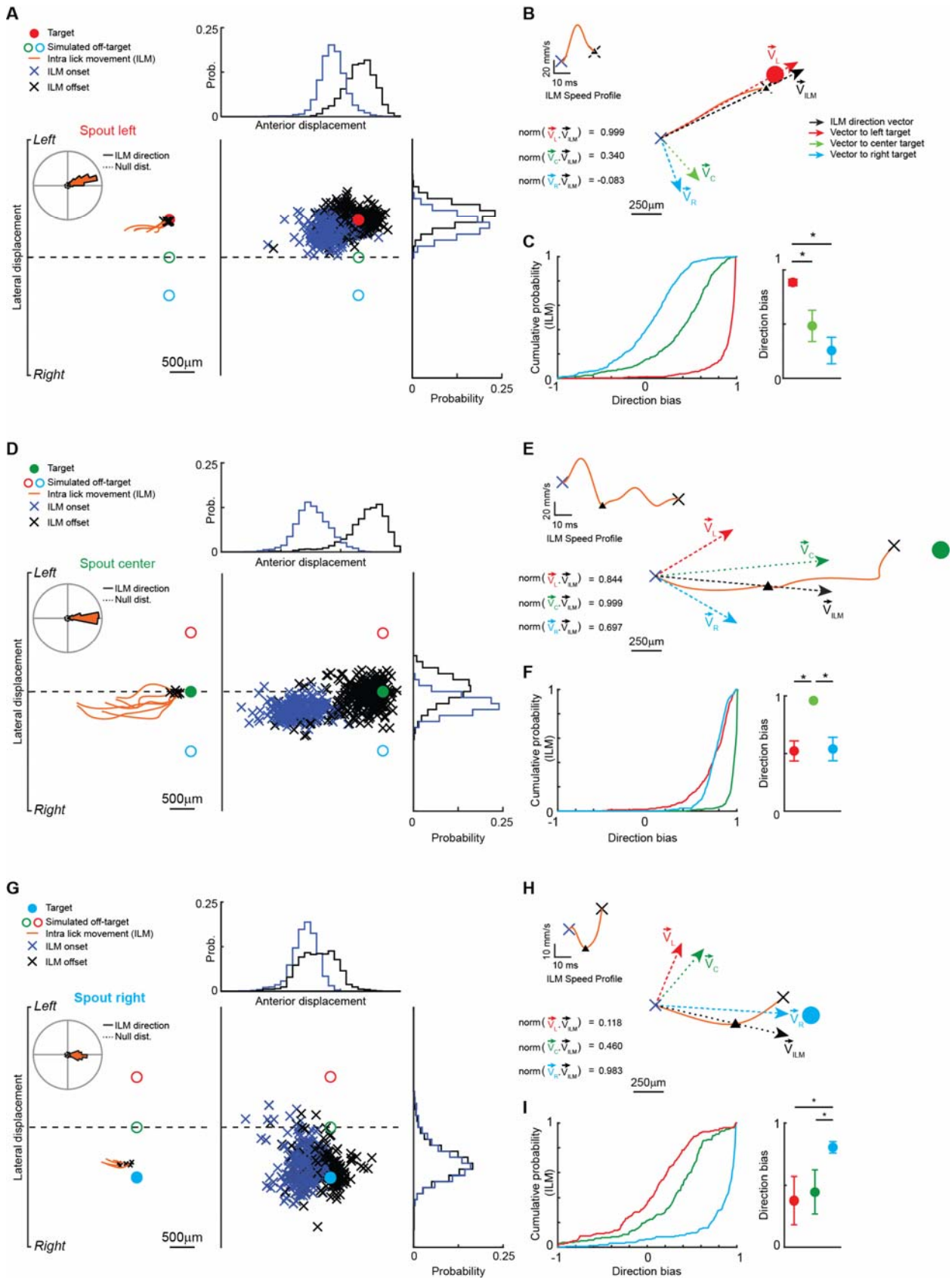
A
Target
Simulated off-target
Intra lick movement (ILM)
ILM onset
ILM offset
Spout left
Left
Right
ILM direction
Null dist.
Lateral displacement
500μm
Prob.
Anterior displacement
Probability
B
20 mm/s
10 ms
ILM Speed Profile
norm($\vec{V}_L$,$\vec{V}_{ILM}$) = 0.999
norm($\vec{V}_C$,$\vec{V}_{ILM}$) = 0.340
norm($\vec{V}_R$,$\vec{V}_{ILM}$) = -0.083
ILM direction vector
Vector to left target
Vector to center target
Vector to right target
250μm
C
Cumulative probability (ILM)
Direction bias
D
Spout center
E
norm($\vec{V}_L$,$\vec{V}_{ILM}$) = 0.844
norm($\vec{V}_C$,$\vec{V}_{ILM}$) = 0.999
norm($\vec{V}_R$,$\vec{V}_{ILM}$) = 0.697
F
G
Spout right
H
norm($\vec{V}_L$,$\vec{V}_{ILM}$) = 0.118
norm($\vec{V}_C$,$\vec{V}_{ILM}$) = 0.460
norm($\vec{V}_R$,$\vec{V}_{ILM}$) = 0.983
I

Fig. 4. Intra-lick movements are directionally biased towards remembered spout locations.
(A-C) ILM kinematics for spout-left sessions.
A) Left: Six representative ILMs and polar plot direction distribution of all ILMs produced in a single spout-left session (inset). Middle: Scatter plot of tongue tip positions at protrusion offset (blue) and retraction onset (black), indicating ILM start and end points. Probability distributions of the ILM start- and end-points are projected along the axes at top and right (binsize,120um).
B) Example of a single ILM path and its speed profile (orange). The ILM's initial direction (V_{ilm}, black dotted line) was computed from the vector connecting ILM starting point to its position at the first speed minimum (upward black triangle in speed and path plots). The dot products between this ILM direction vector and three additional vectors from ILM starting point to left, center, and right targets (dotted red, green, and blue lines, respectively) were computed to quantify the 'direction bias', the extent to which a given ILM was aimed at each of the three candidate targets.
C) Left: Cumulative distributions of directional biases for all ILMs produced in a single session to the three candidate targets (colored as in B). ILMs were reliably aimed to the left target. Right: Directional biases of ILMs to left, center, and right targets spout-left sessions (median +/- IQRs across n=9, 9 and 7 animals respectively)
(D-F) ILM kinematics for spout-center sessions, plotted as in A-C.

(G-I) ILM kinematics for spout-right sessions, plotted as in A-C.

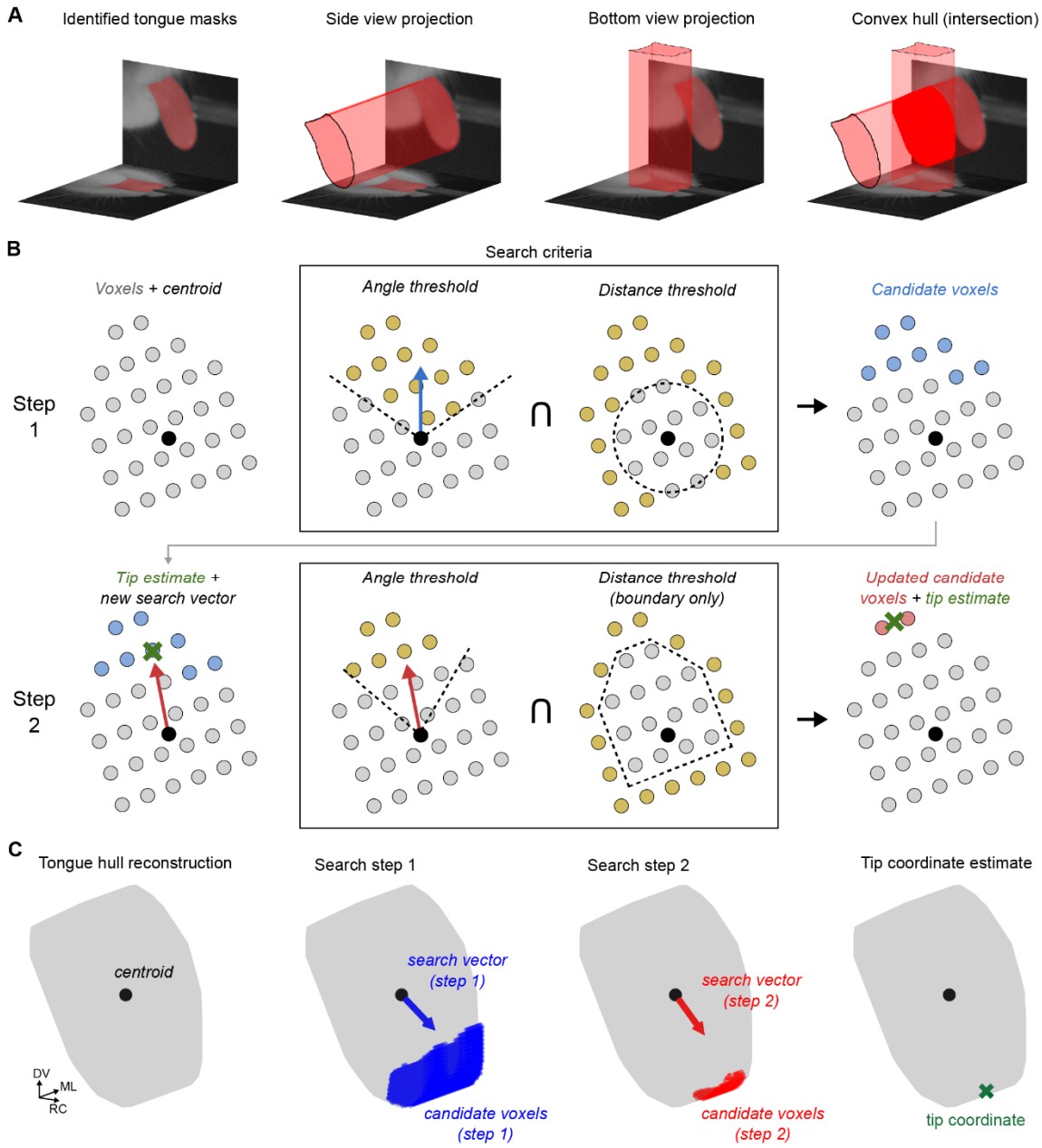

Fig. S1. Method for extracting 3D tongue tip kinematics.

(A) An example of the process used to generate a 3D voxel hull from the two views of the mouse tongue. The walls of the diagrams are stills taken from the high-speed video, with the segmented tongue mask highlighted in red. The final hull (rightmost diagram) is obtained by identifying the intersection of the projections of the side and bottom view tongue masks. (B) A 2D illustration of the tip coordinate search. With the voxels (gray circle) and centroid (black circle) identified, the first search step is performed, in which candidate voxels (blue) are found via the intersection of voxels satisfying the two search criteria (yellow), namely thresholds on the maximum angle made with the search vector (blue arrow) and the minimum distance from the tongue centroid. These first candidate voxels are then used to generate a refined search vector (red arrow, second row) for the second step of the search. Using this refined search vector, a similar set of angle and

distance thresholds are applied, to determine a refined set of candidate voxels, which are then averaged to determine the tip location. (C) Example of the tip search process with real data in 3D. The gray object is the 3D tongue hull, with the centroid labelled by a black circle. The first search step identifies a set of candidate voxels (blue) that are used to generate a refined search vector for the second search step (red). Using the second step candidate voxels, the tongue tip location is estimated (green ‘x’).

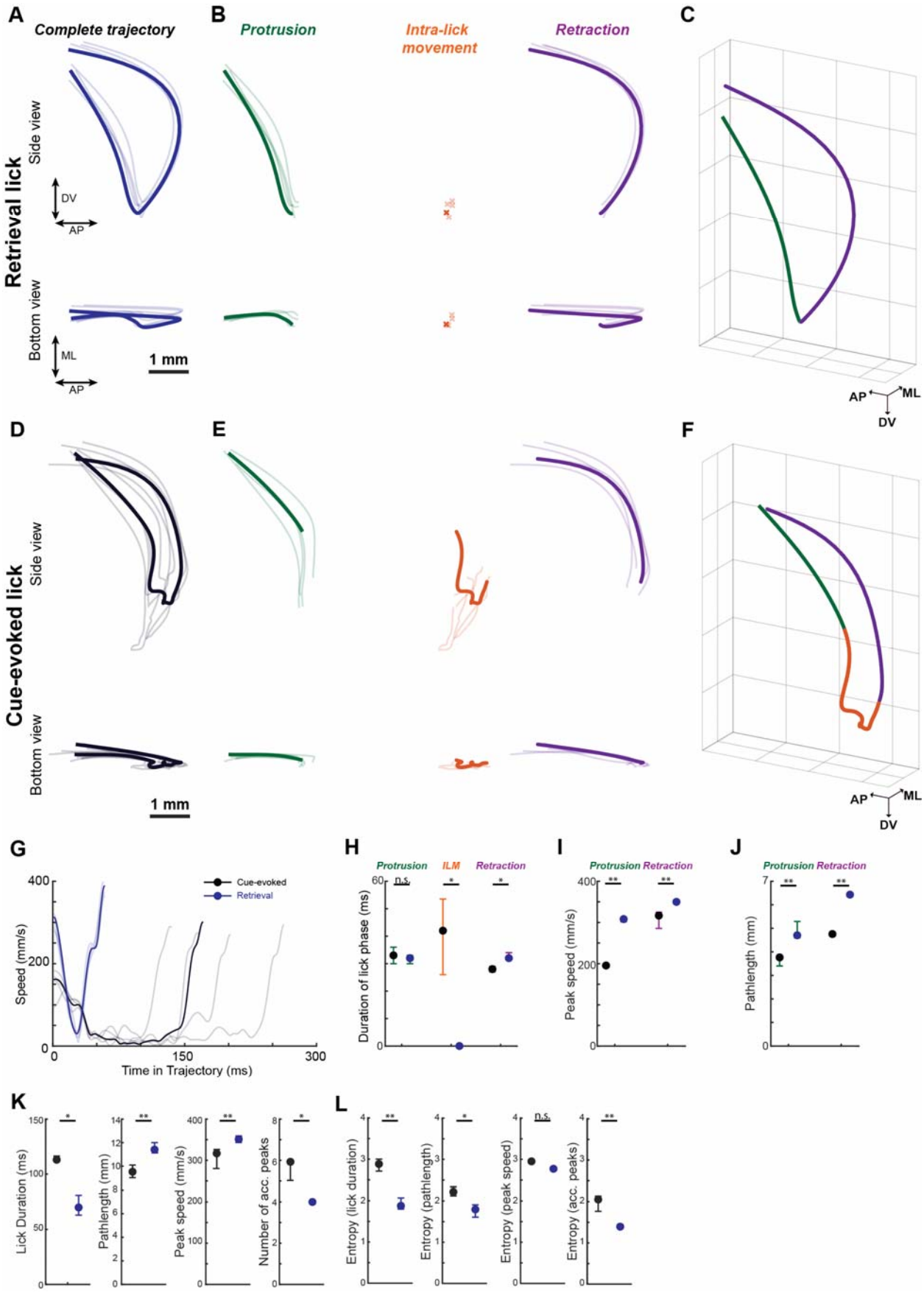
A
Complete trajectory
B
Protrusion
Intra-lick movement
Retraction
C
Retrieval lick
Side view
DV
AP
Bottom view
ML
AP
1 mm
AP
ML
DV
D
E
F
Cue-evoked lick
Side view
Bottom view
1 mm
AP
ML
DV
G
Cue-evoked
Retrieval
Speed (mm/s)
Time in Trajectory (ms)
H
Protrusion
ILM
Retraction
n.s.
Duration of lick phase (ms)
I
Protrusion
Retraction
Peak speed (mm/s)
J
Protrusion
Retraction
Pathlength (mm)
K
Lick Duration (ms)
Pathlength (mm)
Peak speed (mm/s)
Number of acc. peaks
L
Entropy (lick duration)
Entropy (pathlength)
Entropy (peak speed)
n.s.
Entropy (acc. peaks)

Fig. S2. Water retrieval and cue-evoked licks exhibit distinct kinematics

A-C) Water retrieval licks, defined as those initiated after spout contact.

A) Six overlaid tongue tip trajectories during retrieval licks. A single lick is bold for clarity. B) Protrusion, intra-lick, and retraction phases of the trajectories from A are separately plotted. Orange X symbols denote the absence of ILMs.

C) 3-D trajectory of the highlighted lick shown in A, with protrusion (green) and retraction (purple) lick phases indicated.

D-F) Data plotted as in A-C showing cue-evoked licks. Note the prominent ILMs.

G) Speed versus time for the retrieval (blue) and cue-evoked (black) tongue trajectories shown in A,D.

H-J) Median durations (H), Peak speeds (I) and Pathlengths (J) of lick phases during cue-evoked (black) and retrieval (blue) licks. (Median ± IQRs across 9 animals).

K-L) Kinematics (K) and entropy (L) of lick durations, pathlengths, peak speeds, and number of acceleration peaks (median± IQR across animals)

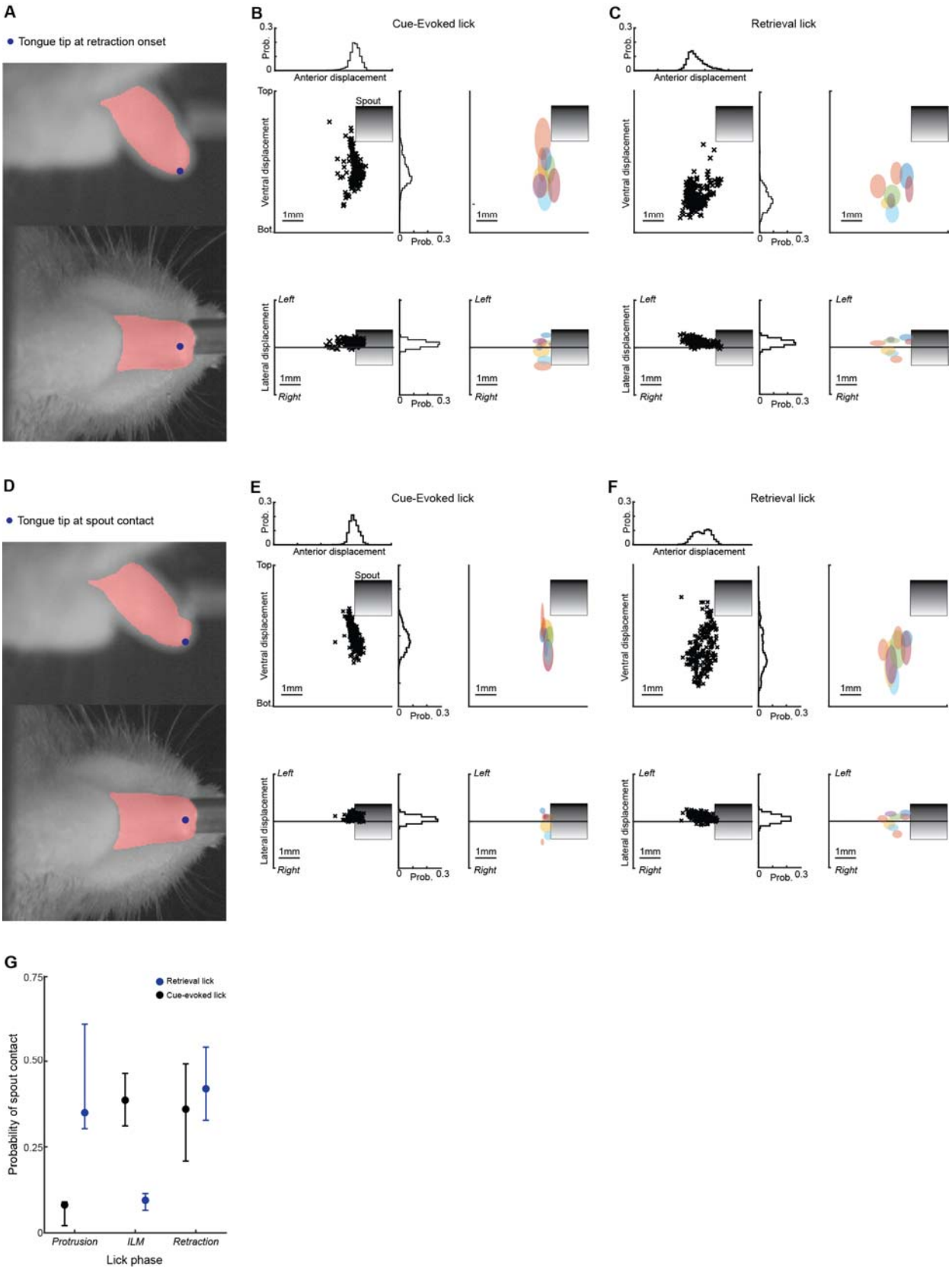
A
Tongue tip at retraction onset
B
Cue-Evoked lick
C
Retrieval lick
Anterior displacement
Prob.
Top
Bot
Spout
Ventral displacement
Lateral displacement
Left
Right
1mm
D
Tongue tip at spout contact
E
Cue-Evoked lick
F
Retrieval lick
G
Retrieval lick
Cue-evoked lick
Probability of spout contact
Protrusion
ILM
Retraction
Lick phase

Fig. S3. Tongue tip positions at the moment of retraction onset and spout contact

A) Side and bottom views of the tongue at the moment of retraction onset.

B) Scatter plots of tongue tip positions at retraction onset for side (top) and bottom views (bottom) during successful cue-evoked licks. Note that for cue-evoked licks retraction onsets are identical positions as ILM offset. Probability distributions are projected along the axes at top and right (binsize, 120um). Right: 2-D standard deviations of tongue tip positions at retraction onset for 9 mice (each mouse independently color-coded). Note that each mouse exhibits a 'preferred' target location for retraction onset.

C) Data plotted as in B for retrieval licks.

D-F) Data plotted as in A-C for tongue tip positions at the moment of spout contact

G) Probability of spout contact as a function of the distinct lick phases for cue evoked and water retrieval licks (blue and black, respectively)

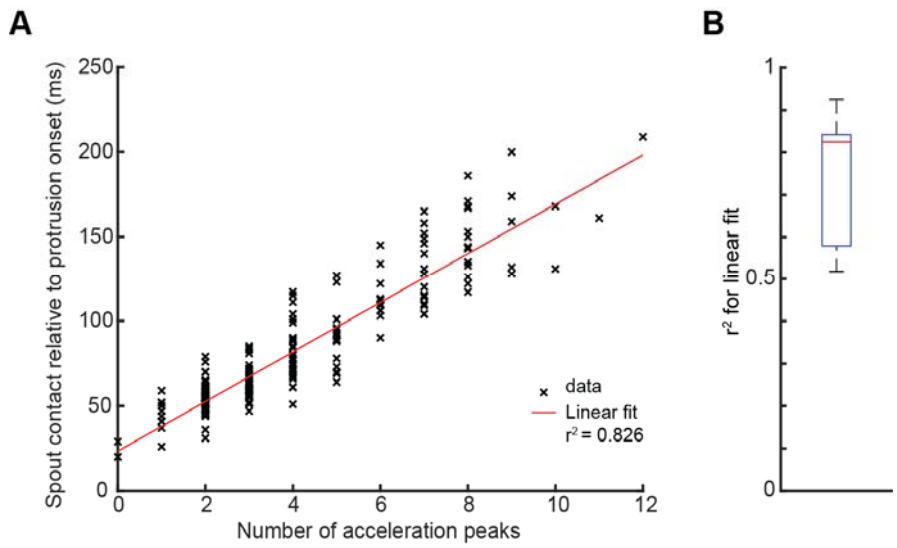

Fig. S4. The number of acceleration peaks per lick predicts latency to spout contact
A) The latency to spout contact relative to protrusion onset is plotted against the number of acceleration peaks per lick from a single session. Red line, linear fit.
B) Boxplot showing r2 for linear fits across 9 animals (red line: median; box edges: IQR; whiskers: 95% CI).

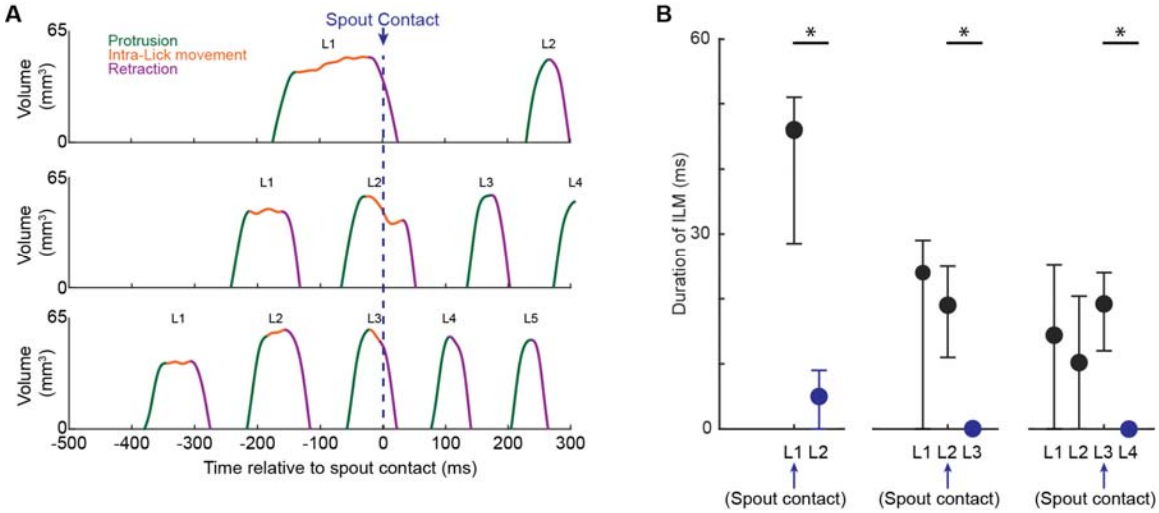

Fig. S5. Spout contact transforms the kinematics of subsequent licks.
A) Tongue volumes as a function of time during three trials where first spout contact occurred on the first, second, or third lick. Note that licks initiated before spout contact exhibited substantial ILMs, whereas those initiated after spout contact lacked ILMs.
B) Duration of the ILM lick phase as a function of lick number in cases where first spout contact happened on first, second, or third licks (median ± IQR across animals n= 9 (first), 9 (second) and 6 (third lick) animals). Spout contact reliably transformed the kinematics of subsequently initiated licks.

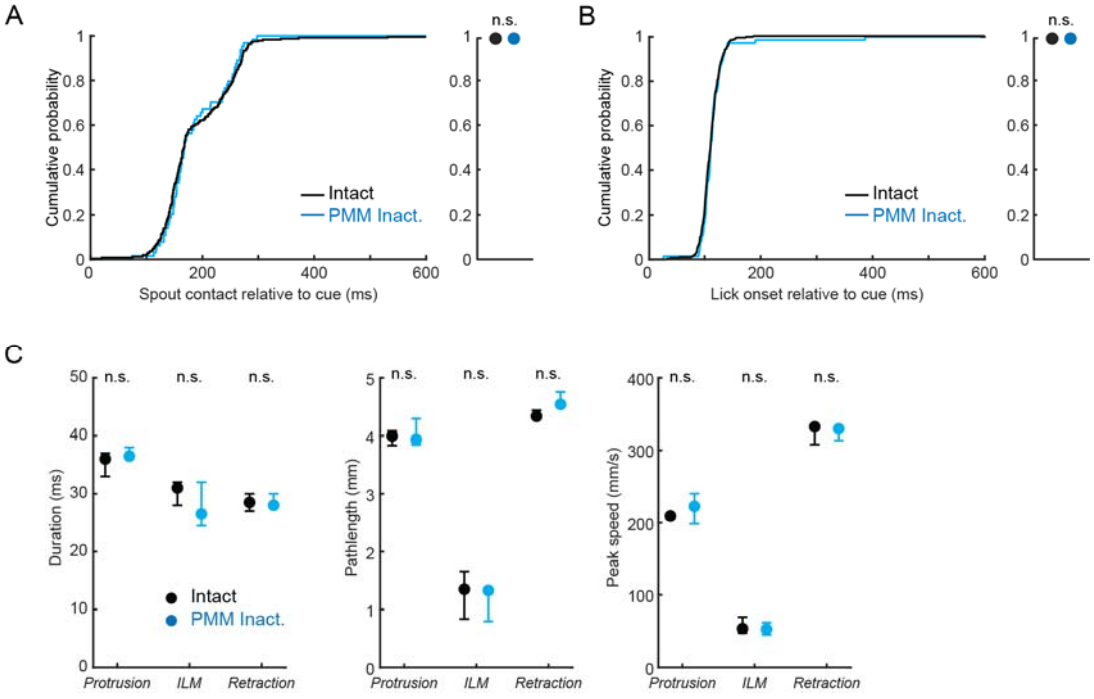

Fig. S6. Inactivation of PMM does not impact task performance or lick kinematics
A) Cumulative probability of tongue-spout contact relative to cue onset during laser-off and PMM-photoinactivated trials. Right, median ± IQR probability of spout contact within a trial across mice (n = 9 mice).
C) Median durations, Pathlengths, and Peak speeds for all lick phases with PMM intact (black) and PMM Inactivated (blue). (median ± IQRs).

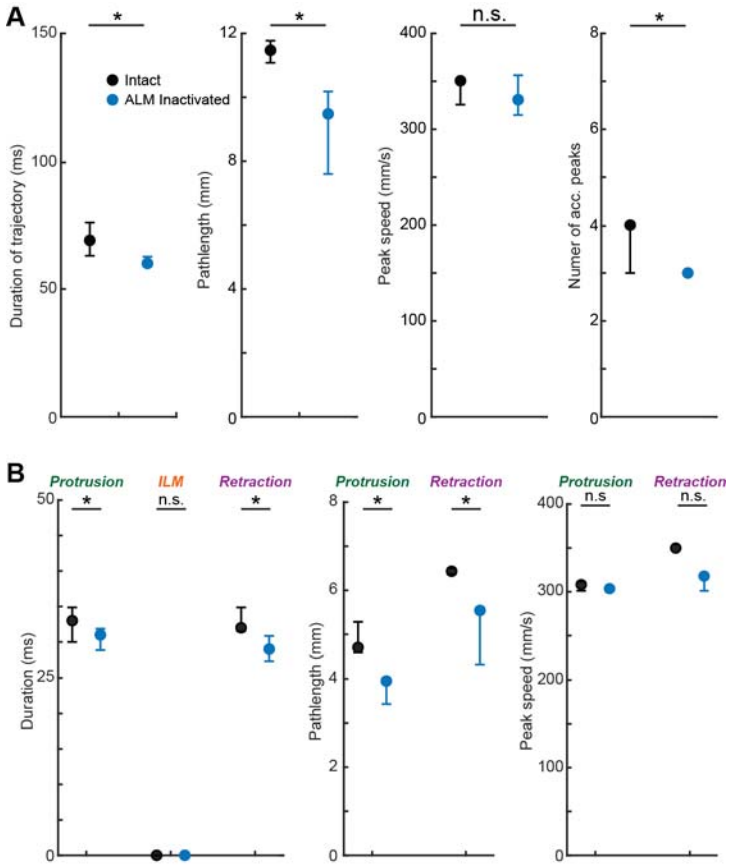

Fig. S7. ALM photoinhibition resulted in hypometric retrieval licks

A) Median durations, Pathlengths, Peak speeds and number of accleration peaks during retrieval licks produced with ALM intact and inactivated (black and blue, respectively).

B) Median durations, Pathlengths, and Peak speeds for protrusion and retraction phases of retrieval licks with ALM intact (black) and ALM Inactivated (blue). (median ± IQRs). Note that these licks lacked ILMs (n = 7 animals)

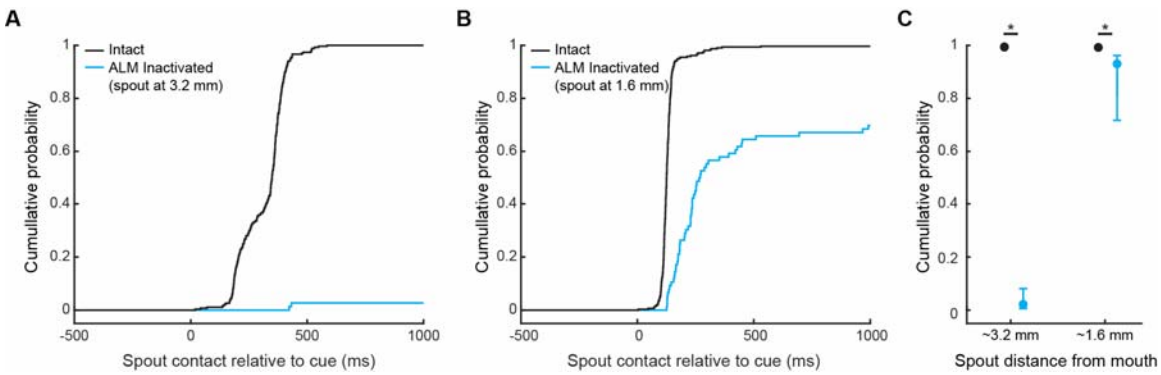

Fig. S8. Proximal spout placement rescues ALM inactivation-associated spout contact deficits

(A-B) Cumulative probability of spout contact relative to cue onset for ALM intact (black) and inactivated (blue) trials in sessions where the spout was 1.6 mm (A) and 3.2 mm (B) from the incisors. C) Median probability of spout contact across animals from spout-close and spout-far sessions.